Molecular Biology of the Cell
Vol. 20, 1937–1948, April 1, 2009

Vps41 Phosphorylation and the Rab Ypt7 Control the Targeting of the HOPS Complex to Endosome–Vacuole Fusion Sites

Margarita Cabrera,* Clemens W. Ostrowicz,* Muriel Mari,† Tracy J. LaGrassa,*‡ Fulvio Reggiori,† and Christian Ungermann*

*Biochemistry Section, Department of Biology, University of Osnabrück, 49076 Osnabrück, Germany; and †Department of Cell Biology and Institute of Biomembranes, University Medical Centre Utrecht, 3584 CX Utrecht, The Netherlands

Submitted September 17, 2008; Revised January 22, 2009; Accepted January 23, 2009
Monitoring Editor: Jean E. Gruenberg

Membrane fusion depends on multisubunit tethering factors such as the vacuolar HOPS complex. We previously showed that the vacuolar casein kinase Yck3 regulates vacuole biogenesis via phosphorylation of the HOPS subunit Vps41. Here, we link the identified Vps41 phosphorylation site to HOPS function at the endosome–vacuole fusion site. The nonphosphorylated Vps41 mutant (Vps41 S-A) accumulates together with other HOPS subunits on punctate structures proximal to the vacuole that expand in a class E mutant background and that correspond to in vivo fusion sites. Ultrastructural analysis of this mutant confirmed the presence of tubular endosomal structures close to the vacuole. In contrast, Vps41 with a phosphomimetic mutation (Vps41 S-D) is mislocalized and leads to multilobed vacuoles, indicative of a fusion defect. These two phenotypes can be rescued by overproduction of the vacuolar Rab Ypt7, revealing that both Ypt7 and Yck3-mediated phosphorylation modulate the Vps41 localization to the endosome–vacuole junction. Our data suggest that Vps41 phosphorylation fine-tunes the organization of vacuole fusion sites and provide evidence for a fusion "hot spot" on the vacuole limiting membrane.

INTRODUCTION

Membrane dynamics in the endomembrane system of eukaryotic cells is achieved by controlled fission and fusion events that determine protein sorting and organelle identity. Transport vesicles that are generated with the help of coat proteins allow the exchange of lipids and proteins between subcellular compartments. Upon recognition at the target organelle, vesicles discharge their content by fusing with the organelle lipid bilayer.

Three central players control the fusion reaction: Rab GTPases, tethering factors, and soluble *N*-ethylmaleimide-sensitive factor attachment protein receptors (SNAREs) (Cai *et al*., 2007). Rab GTPases are molecular switches that are activated by guanine nucleotide exchange factors (GEFs) and bind their effector-tethering factors in the active guanosine triphosphate (GTP)-form. Due to their low intrinsic GTPase activity, inactivation requires GTPase-activating proteins (GAPs) (Bos *et al*., 2007). Tethering factors that bind to the Rab-GTP come in two flavors. Long tethers, found predominantly at endosomes and the Golgi, contain coiled-coil domains and bridge long distances to capture vesicles (Drin *et al*., 2008). Multimeric tethering complexes consist of up to 10 subunits with distinct activities and can be assigned to transport steps between organelles. The exocyst (eight subunits) promotes fusion of exocytic vesicles with the plasma membrane, GARP (four subunits) is responsible for fusion of endosome-derived vesicles with the Golgi, COG (eight subunits) operates within the Golgi, and TRAPP I and II (7 and 10 subunits, respectively) operate at the endoplasmic reticulum (ER)-Golgi and intra-Golgi interface (Whyte and Munro, 2002; Cai *et al*., 2007; Markgraf *et al*., 2007).

Our laboratory focuses on fusion reactions at endosomes and the vacuole (LaGrassa and Ungermann, 2005; Ostrowicz *et al*., 2008; Peplowska *et al*., 2007). At the late endosome, we could identify the CORVET complex as an effector of the Rab5-homologue Vps21 (Peplowska *et al*., 2007), whereas the homologous HOPS complex binds to Ypt7 (yeast Rab7) in its GTP-form to promote fusion at the vacuole (Seals *et al*., 2000; Stroupe *et al*., 2006; Starai *et al*., 2008). The HOPS complex consists of six subunits. The class C Vps11, Vps16, Vps18, and Vps33 subunits, named after the strongly fragmented vacuole phenotype of the corresponding deletion mutant (Raymond *et al*., 1992; Rieder and Emr, 1997), are present in both the HOPS and CORVET complexes (Peplowska *et al*., 2007). Vps11 and Vps18 have C-terminal RING domains (Rieder and Emr, 1997), and Vps33 has homology to Sec1/Munc18 proteins. However, none of the class C subunits has been linked to a specific function except complex integrity. In contrast, the specific HOPS subunit Vam6/Vps39 has nucleotide exchange activity (Wurmser *et al*., 2000), and we have recently obtained evidence that the other specific component Vps41/Vam2 is the effector subunit of the complex (Ostrowicz and Ungermann, unpublished data). In addition, Vps41 is required for the biogenesis of adapter protein complex 3 (AP-3) vesicles that transport proteins directly from

This article was published online ahead of print in *MBC in Press* (http://www.molbiolcell.org/cgi/doi/10.1091/mbc.E08–09–0943) on February 4, 2009.

‡ Present address: Jones Day, 222 East 41st St., New York, NY 10017.

Address correspondence to: Christian Ungermann (christian.ungermann@biologie.uni-osnabrueck.de).

the Golgi to the vacuole (Rehling *et al*., 1999). Importantly, Vps41 becomes phosphorylated at the vacuole by the casein kinase 1 Yck3 (LaGrassa and Ungermann, 2005). In *yck3*Δ cells, Vps41 accumulates in distinct puncta adjacent to or on the vacuolar membrane in vivo, and *yck3*Δ vacuoles are less sensitive to Ypt7 inhibitors than wild-type vacuoles in the in vitro vacuole fusion reaction. If Yck3 is overproduced or cells are challenged by osmotic shock, Vps41 phosphorylation is clearly observed in vivo. In addition, we observed a faster recovery of in vivo fusion in *yck3*Δ cells under highly osmotic conditions (LaGrassa and Ungermann, 2005).

Because we could not exclude an indirect effect of Yck3 on Vps41 due to phosphorylation of other putative substrates, we decided to identify the specific Yck3 phosphorylation sites in Vps41 and analyze the consequences of the corresponding mutations. We now show that Vps41 phosphorylation can be linked to its function at the endosome-vacuole interface.

MATERIALS AND METHODS

Yeast Strains and Molecular Biology

Yeast strains used are listed in Supplemental Table S1. Yeast strains were cultured in YPD medium, except where indicated. Deletions and tagging of genes with green fluorescent protein (GFP) or tandem affinity purification (TAP) tags were performed using homologous recombination of polymerase chain reaction (PCR)-amplified fragments (Puig *et al*., 1998; Janke *et al*., 2004). For the expression of Vps41 under the *NOP1* promoter, the *VPS41* open reading frame was amplified by PCR and inserted into the integrative vector pRS406 containing the *NOP1* promoter. The resulting pRS406-*NOP1*pr-*VPS41* plasmid was transformed into *vps41*Δ strains. Point mutations in *VPS41* were generated using the QuickChange site-directed mutagenesis kit from Stratagene (La Jolla, CA). The vector coding for the TBC domain of Gyp1, pET22-Gyp1-46 (Wang *et al*., 2003), was transformed into BL21 Rosetta. Protein expression was induced by addition of 0.5 mM isopropyl β-D-thiogalactoside overnight at 16°C. Purification was performed using the nickel-nitrilotriacetic acid resin (QIAGEN, Hilden, Germany) and elution with 300 mM imidazole. Buffer exchange to 20 mM piperazine-*N*,*N*′-bis(2-ethanesulfonic acid)/KOH, pH 6.8, 200 mM sorbitol was performed with a PD10 column (GE Healthcare, Munich, Germany).

Microscopy

For GFP microscopy, yeast cells were grown to mid-log phase in YPD or selective medium, collected by centrifugation, washed once with SDC medium supplemented with all amino acids, and immediately analyzed by fluorescence microscopy. Staining of the cells with *N*-[3-triethylammoniumpropyl]-4-[*p*-diethylaminophenylhexatrienyl] pyridinium dibromide (FM4-64) was performed as described previously (LaGrassa and Ungermann, 2005). Briefly, cells were incubated with 30 μM FM4-64 for 30 min, washed with medium, and chased for 1 h. To visualize class E compartment, SEY6210 cells were incubated with 30 μM FM4-64 for 15 min and chased for 45 min. Images were acquired with a Leica DM5500 B microscope equipped with a SPOT Pursuit camera using GFP, FM4-64 and differential interference contrast (DIC) filters, and pictures were processed using Adobe Photoshop CS3 (Adobe Systems, Mountain View, CA).

Electron Microscopy (EM) Analysis

Strains were grown to exponential phase before being processed for electron microscopy. Permanganate fixation, dehydration, and embedding in Spurr's resin were carried out as described previously (Griffith *et al*., 2008). Uranyl acetate-stained sections were viewed in a JEOL 1200 transmission electron microscope (JEOL, Tokyo, Japan), and images were recorded on Kodak 4489 sheet films (Eastman Kodak, Rochester, NY).

Yeast Cell Lysis and Membrane Fractionation

Total protein extracts were obtained by cell lysis in 0.25 N NaOH, 140 mM β-mercaptoethanol, 3 mM phenylmethylsulfonyl fluoride or phenylmethanesulfonyl fluoride (PMSF), followed by precipitation with 13% (vol/vol) trichloroacetic acid (TCA) and acetone wash. For subcellular fractionation, strains were grown in 20 ml of YPD cultures to OD_{600} = 1–1.5. Cells were treated with 10 mM DTT followed by an incubation with lyticase for 20 min at 30°C. Spheroplasts were resuspended in 1 ml of lysis buffer (200 mM sorbitol, 50 mM KOAc, 20 mM HEPES-KOH, pH 6,8, 1× protease inhibitor cocktail [PIC]: 0.1 μg/ml leupeptin, 1 mM *o*-phenanthroline, 0.5 μg/ml pepstatin A, 0.1 mM Pefabloc], 1 mM PMSF, and 1 mM dithiothreitol [DTT]) containing 2 μg/ml DEAE-dextran and incubated on ice for 5 min, followed by a 2-min incubation at 30°C. The total extract was centrifuged at 300 × *g* for 3 min at 4°C, and the supernatant (S4) was then centrifuged for 15 min at 20,000 × *g*. The resulting pellets (P20) were centrifuged at 100,000 × *g* for 1 h to obtain pellet (P100) and supernatant (S100) fractions. Alternatively, supernatant (S4) was centrifuged at 13,000 × *g* for 15 min to isolate the pellet (P13) used in Vps41 phosphorylation assay. P13 fractions were diluted to 0.4 mg/ml in PS buffer (20 mM HEPES-KOH, pH 6.8, and 200 mM sorbitol) containing 0.1 × PIC.

Vps41 Phosphorylation Assay

P13 fractions were incubated in 150-μl reaction aliquots for 45 min at 26°C in PS buffer supplemented with salts (0.5 mM $MgCl_2$, 0.5 mM $MnCl_2$, and 125 mM KCl; Mayer *et al*., 1996), 10 μM CoA, and with or without an ATP-regenerating system (0.5 mM ATP, 40 mM creatine phosphate, and 0.1 mg/ml creatine kinase). Membranes were reisolated (10 min at 20,000 × *g* and 4°C), and pellets were resuspended in SDS sample buffer. Vps41 mobility-shift was analyzed by Western blotting.

Vacuole Isolation and Fusion Reaction

Vacuoles were isolated from the yeast strains BJ3505 (*pep4*Δ *prb1*Δ) and DKY6281 (*pho8*Δ) by DEAE-dextran lysis and Ficoll density gradient flotation (Haas, 1995). Vacuoles were diluted to 0.3 mg/ml in PS buffer containing 0.1 × PIC. Vacuole fusion was measured by a biochemical complementation assay as described previously (Haas, 1995). Standard fusion reactions contained 3 μg each of BJ and DKY vacuoles and were incubated for 90 min at 26°C in 30 μl of PS buffer supplemented with salts (5 mM $MgCl_2$ and 125 mM KCl), 10 μM CoA, 0.01 μg of His-Sec18, with or without an ATP-regenerating system. Recombinant Gyp1 was added from a stock at 0.3 μg/μl. The *p*-nitrophenyl phosphate, a colorimetric substrate for the alkaline phosphatase, was added to detergent-solubilized reactions, and the alkaline phosphatase activity was determined by measuring the absorbance of the generated nitrophenol at 400 nm. The results are expressed by subtracting the signal from an incubation lacking ATP.

TAP-Tag Protein Purification

Vps41-TAP purification was performed as described previously (Rigaut *et al*., 1999). Three liters of BJ3505 cell culture was grown at 30°C to OD_{600} = 3–5 and harvested by centrifugation. Cells were then lysed in the following buffer: 50 mM HEPES/KOH, pH 7.4, 300 mM NaCl, 0.15% NP-40 (Igepal CA-630; Sigma-Aldrich, St. Louis, MO), 1.5 mM $MgCl_2$, 1 × FY protease inhibitor mix (Serva, Heidelberg, Germany), 0.5 mM PMSF, and 1 mM DTT. Cell lysates were centrifuged at 100,000 × *g* for 1.5 h and incubated with immunoglobulin G (IgG) beads for 1 h at 4°C. Beads were then washed with 20 ml of lysis buffer supplemented with 0.5 mM DTT and proteins eluted by incubation overnight at 4°C in presence of 7 μl of 1 mg/ml tobacco etch virus (TEV) protease in 150 μl of lysis buffer containing 0.5 mM DTT.

Gel Filtration

TEV eluate was centrifuged for 10 min at 20,000 × *g*, and the supernatant was applied to a Superose 6 10/300 column, connected to an ÄKTA-FPLC-System (GE Healthcare) that had been equilibrated with two column volumes of the previous lysis buffer without protease inhibitors but containing 4 mM DTT. The flow rate was set to 0.3 ml/min, and 24 fractions of 1 ml were collected. For protein detection, fractions 6–19 were TCA precipitated and loaded onto a 4–12% SDS-polyacrylamide gel electrophoresis (PAGE) gradient gel (NuPAGE; Invitrogen, Carlsbad, CA).

RESULTS

Ultrastructural Analysis of yck3Δ Cells

In *yck3*Δ cells, GFP-Vps41 accumulates in vivo in distinct punctate structures adjacent to the vacuole (LaGrassa and Ungermann, 2005) (Figure 1A). This observation prompted us to analyze *yck3*Δ cells by electron microscopy. In contrast to wild-type cells, *yck3*Δ cells contain elongated structures proximal to the vacuole (Figure 1B, A and B), which are in part reminiscent of the class E endosomes observed upon loss of ESCRT subunits (Rieder *et al*., 1996). The tubular structures may correspond to several flat endosomal cisternae that seem to be stacked onto each other (Figure 1B, C–E). Some structures look like open cups, which may be a result of the cutting procedure (Figure 1B, F–H). We consider it likely that the prominent GFP-Vps41 fluorescence signal corresponds to these stacked structures and those could be late endosomal compartments. This idea is supported by the fact that in *yck3*Δ cells, we observed colocalization between

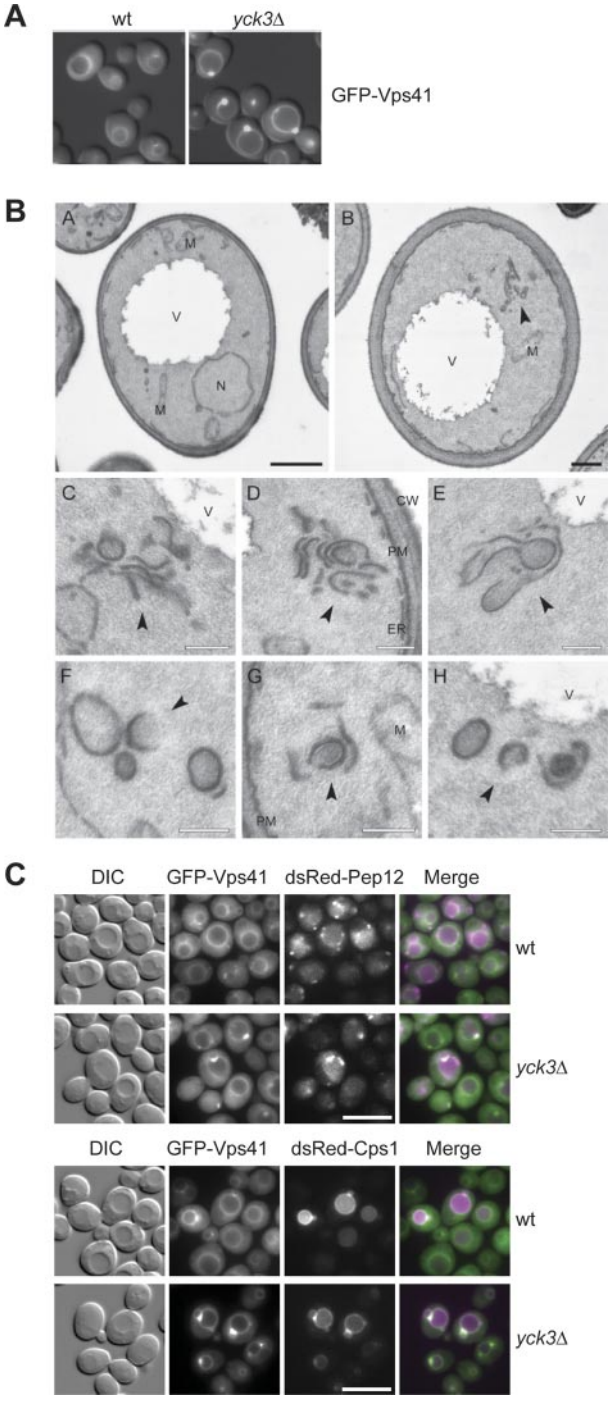

Figure 1. EM analysis of *yck3*Δ cells. (A) Localization of GFP-tagged Vps41. The SEY6210 wild-type and *yck3*Δ cells expressing N-terminally GFP-tagged Vps41 were analyzed by fluorescence microscopy. Overlays between DIC and GFP images are shown. (B) The SEY6210 *GFP-VPS41* (A) and SEY6210 *GFP-VPS41 yck3*Δ (B–H) strains were grown to exponential phase and embedded in Spurr's resin as described in *Materials and Methods*. Arrowheads in B–H point to the anomalous membranous conformations observed in the preparations. C–E highlight the large membranous conformations frequently found adjacent to the vacuole, whereas panels F to H feature the cytoplasmic structures that in most of the cases are circular. N, nucleus; V, vacuole; M, mitochondrion; CW, cell wall; ER, endoplasmic reticulum; PM, plasma membrane. Black bar, 500 nm; white bar 200 nm. (C) Colocalization of GFP-Vps41 with endosomal markers. N-terminally GFP-tagged Vps41 and dsRed-tagged Pep12 or Cps1 were visualized by fluorescence microscopy in SEY6210 wild-type and *yck3*Δ cells. Bar, 10 μm.

GFP-Vps41 and both the endosomal SNARE Pep12 and the cargo protein Cps1 that is sorted to the vacuole via endosomes (Figure 1C).

Identification of the Yck3 Phosphorylation Site

One fundamental problem of our EM analysis is the correlation of the altered endosomal morphology to the function of Vps41 because Yck3 has several other targets within the cell, for example, Vam3 (Brett *et al*., 2008). To unequivocally link the in vivo and in vitro effects observed in the *yck3*Δ mutant to Vps41 function, we searched for the phosphorylation sites in the protein. The Vps41 phosphorylation results in a size shift on gels and is observed in vitro if vacuole-containing membranes are incubated in the presence of ATP (Figure 2A). The Vps41 size shift is also detected in vivo but requires the addition of phosphatase inhibitors during cell lysis (LaGrassa *et al*., 2005; our unpublished observations). Although the deletion of several vacuolar or endosomal proteins involved in fusion did not interfere with Vps41 phosphorylation, any mutation causing Yck3 missorting, such as the truncation of the Yck3 C-terminal domain, abolished Vps41 phosphorylation (Figure 2B and Supplemental Figure S1; Sun *et al*., 2004). To identify the phosphorylation site, we screened available databases for casein kinase I sites within the Vps41-sequence (Netphos, http://www.cbs.dtu.dk/services/NetPhos/; Scansite, http://scansite.mit.edu/) and identified four possible consensus sequences (Figure 2C). The relevant serine and threonine residues were changed into alanines in different combination and the resulting Vps41 mutant forms were expressed in the *vps41*Δ background. We then purified membrane fractions and tested for an ATP-dependent mobility shift on SDS-PAGE gels (Figure 2D). Mutations within two regions of Vps41, starting at positions 118 and 364, blocked phosphorylation. Because the deletion of *YCK3* results in large vacuoles (LaGrassa and Ungermann, 2005), we tested for vacuole morphology and observed that only the S364, 367, 368, 371, 372A, T376A mutant mimicked the *yck3*Δ phenotype and was also located on the vacuolar rim (Figure 2E), whereas the S118, 120, 121A mutant showed fragmented vacuoles indicating a loss-of-function (data not shown). Further analysis of this phosphorylation site by the in vitro phosphorylation assay revealed that the double mutant S367, 368A had reduced mobility shift and the mutations S371,372A impaired Vps41 phosphorylation (Figure 2F), indicating that they are the main sites. We confirmed these results monitoring in vivo Vps41 phosphorylation (data not shown). We therefore decided to conduct further studies with a quadruple mutant of S367, 368, 371, 372A, which we abbreviated Vps41 S-A in the remaining text (or S-D for the phosphomimetic mutant).

The Vps41 Phosphorylation Status Affects the HOPS Complex Localization

To address the consequences of Vps41 phosphorylation, we analyzed vacuole morphology in our mutant strains. Whereas the Vps41 S-A or *yck3*Δ mutant displayed round vacuoles, the phosphomimetic Vps41 S-D mutant had multilobed vacuoles (Figure 3A). This result is in agreement with our previous studies, which showed that overproduction of Yck3 leads to a decrease in vacuole fusion in vitro, although no fragmentation of vacuoles could be observed in this strain background (LaGrassa and Ungermann, 2005). Consistent with the vacuole morphology phenotype, the GFP-tagged Vps41 S-A mutant localizes to vacuoles and dot-like structures (Figure 3B), resembling wild-type GFP-Vps41 distribution in *yck3*Δ cells (LaGrassa and Ungermann,

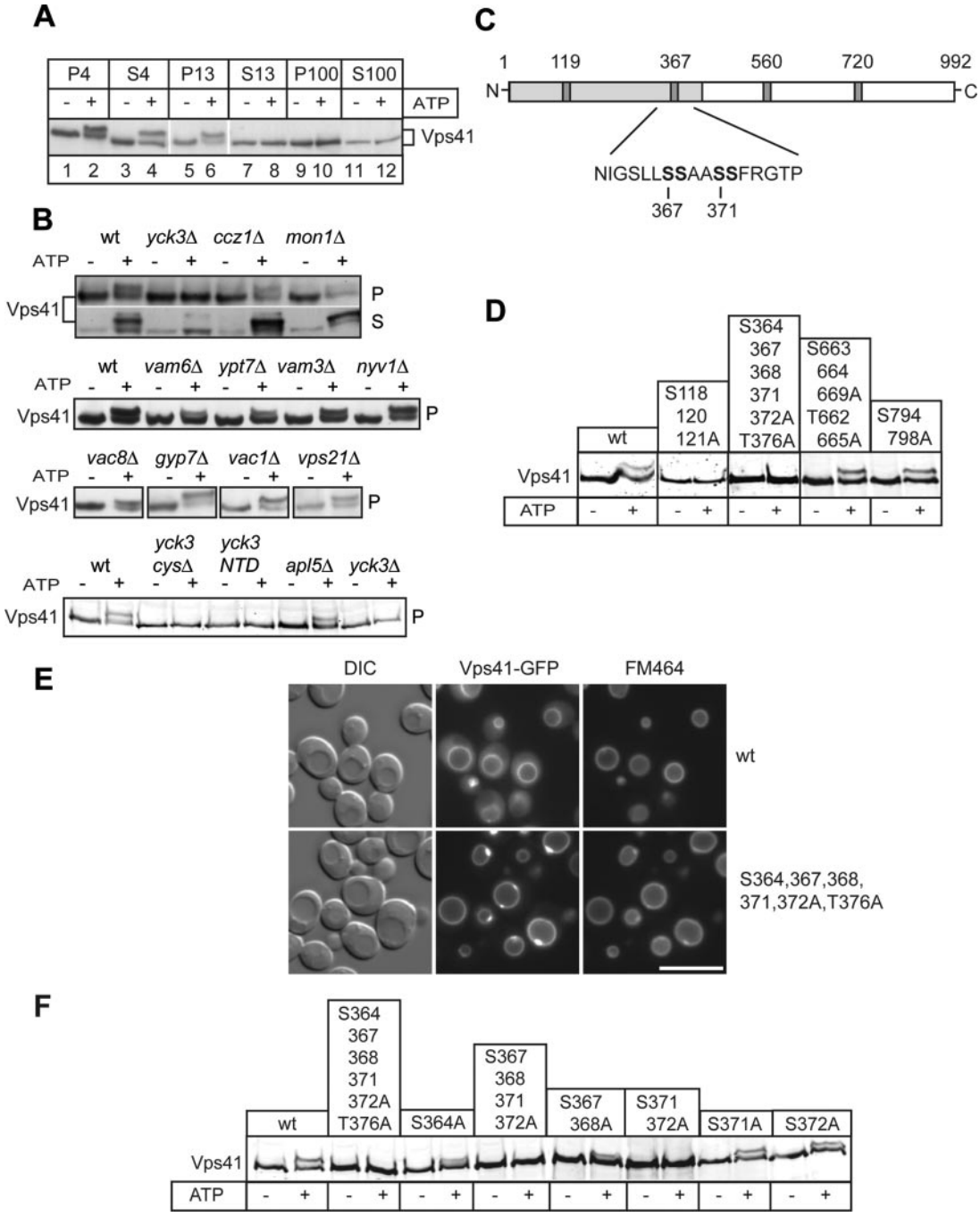

Figure 2. Identification of the Vps41 phosphorylation site. (A) Phosphorylation of Vps41 occurs on membranes. Yeast cells were separated by subcellular fractionation into a low-speed (P4), a medium-speed (P13), and a high-speed pellet (P100). Pellets and the corresponding supernatants (S4, S13, and S100) were incubated for 60 min in the absence or presence of ATP and analyzed by SDS-PAGE and Western blotting using an anti-Vps41 antiserum. (B) Proteins influencing Vps41 phosphorylation. Membranes (P13) obtained from the indicated yeast deletion mutants were incubated without and with ATP and analyzed as described in A. In the Yck3 *cys*Δ, the C-terminal CCCFCC sequence has been removed, in the Yck3 NTD (amino acids 1-333), only the N-terminal domain (NTD) of Yck3 is expressed. (C) Potential casein kinase phosphorylation sites in Vps41. The Yck3 target sequence is highlighted. Sites were identified using the online ProSite software (Expasy, http://expasy.org/prosite/). (D) Screening of Vps41 mutants. Cells expressing the indicated Vps41 variants were treated and analyzed as described in A. (E) Localization of GFP-tagged Vps41 mutants. Wild-type and the mutant form of Vps41 were C-terminally GFP-tagged and expressed in cells. The resulting strains were incubated with FM4-64 to label vacuoles and analyzed by fluorescence microscopy. Bar, 10 μm. (F) Analysis of the Vps41 phosphorylation site. Membrane fractions of Vps41 alanine mutants were analyzed after ATP incubation as described in A.

2005) (Figure 1A). In contrast, the S-D mutant was found partially displaced into the cytoplasm, an observation that we confirmed by subcellular fractionation (Figure 3, B and C). Together, these results are consistent with the idea that Vps41 localization is impacted by its phosphorylation status.

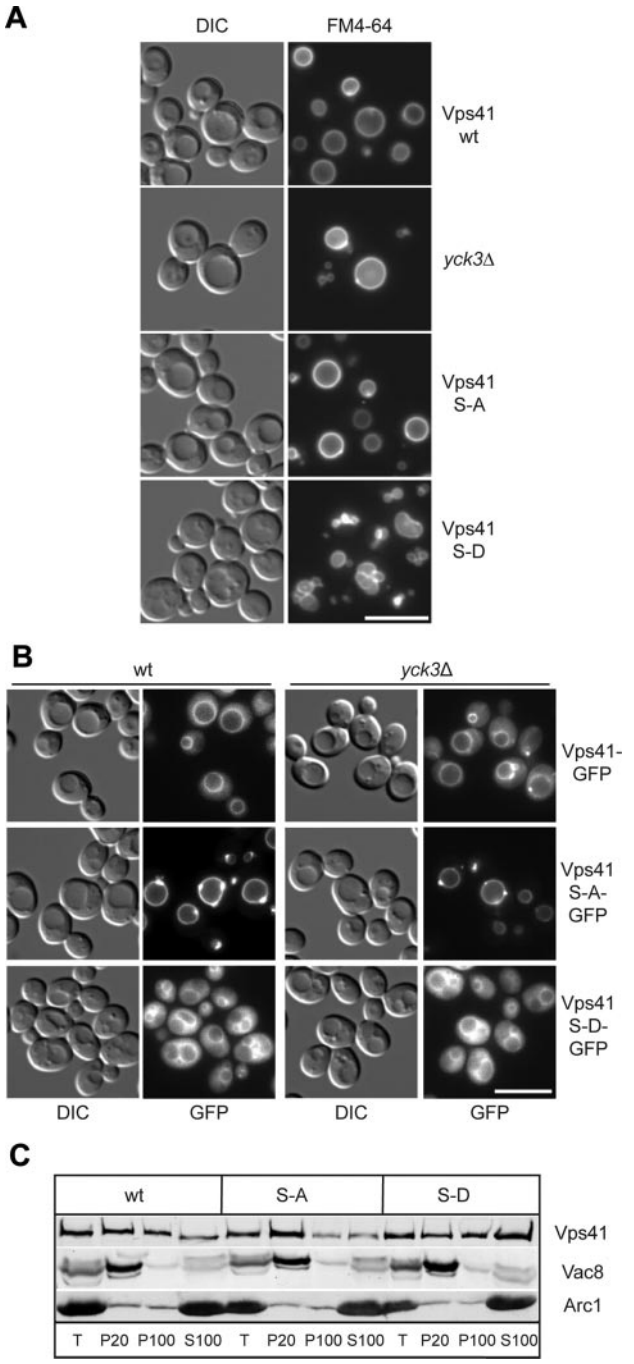

Figure 3. Phosphorylation of Vps41 modulates its localization and function. (A) Vacuole morphology in Vps41 mutants. Strains expressing the indicated Vps41 mutants were incubated with FM4-64 and analyzed by DIC optics or by fluorescence microscopy. Vps41 S-A carries the S367, 368, 371, 372A point mutations, whereas Vps41 S-D contains the comparable phosphomimetic D mutations. Bar, 10 μm. (B) Localization of Vps41 alanine and aspartate mutants in wild-type and *yck3*Δ backgrounds. C-terminal GFP-tagged Vps41 was followed by fluorescence microscopy. Bar, 10 μm. (C) Subcellular fractionation of wild-type and Vps41 mutants. Cells expressing C-terminal GFP-tagged Vps41 wild-type or mutant forms were lysed and separated by centrifugation (20,000 × *g* for 15 min at 4°C) into pellet (P20) and supernatant fractions. The centrifugation of supernatant (100,000 × *g* for 1 h at 4°C) was performed to isolate pellet (P100) and supernatant (S100) fractions. Proteins within each fraction were analyzed by SDS-PAGE and Western blotting using antibodies against Vps41, Vac8, and the cytosolic protein marker Arc1. T = 50% of total protein used for each separation.

To test whether Vps41 phosphorylation status determines the inclusion of this protein in the HOPS complex, we purified TAP-tagged Vps41 variants and the associated proteins by using IgG-Sepharose, and subsequently separated the isolated complexes, which were natively eluted from the IgG beads after TEV protease cleavage, on a gel-filtration column (Figure 4A). As shown previously (Peplowska *et al*., 2007), the assembled HOPS complex is eluted from the column after a volume of 10–11 ml (fractions 10 and 11), whereas monomeric Vps41 is found in fractions 13 and 14. Our analysis revealed that the HOPS complex is copurified with Vps41 regardless of its phosphorylation status. However, we cannot rule out that the association between Vps41 and the HOPS complex differs quantitatively in the different mutant strains. Compared with previous studies (Peplowska *et al*., 2007), we find higher amounts of monomeric Vps41 in our preparations. This is most likely due to the use of a *NOP1* promoter, which leads to higher expression levels of Vps41.

Because Vps41 is involved in vacuole fusion, but it has also been purified in an intermediate complex together with the CORVET subunit Vps3 (Peplowska *et al*., 2007), we decided to determine the localization of GFP-tagged HOPS and CORVET subunits in our mutants. In wild-type cells, Vps11 and Vps18 were found in endosomal dots and on the vacuolar rim, whereas Vam6 localized primarily to the vacuolar rim and to some perivacuolar dots (Figure 4B; Nakamura *et al*., 1997). This accumulation in puncta is enhanced, when the Vps41 S-A mutant was analyzed: All three proteins, Vam6, Vps11, and Vps18, seemed to be enriched in a single dot proximal to or continuous with the vacuolar rim. This distribution is identical to that of the Vps41-GFP S-A mutant (Figure 3B), and it is in agreement with our gel-filtration data indicating that the HOPS complex is assembled in cells expressing the Vps41 S-A variant (Figure 4A). In strong contrast with these observations, GFP-Vam6 was distributed equally along the vacuolar rim in the Vps41 S-D background. Likewise, Vps11 and Vps18 lost their distinct localization and were found on the vacuole and enriched in one or two spots (Figure 4B), which may correspond to endosomes. Statistical analysis of the localization of Vam6, Vps11, and Vps18 in the Vps41 wild type (wt), S-A, and S-D mutant confirmed these conclusions (Figure 4B, bottom). The protein relocalization induced by the Vps41 mutations seems to be exclusively associated to the HOPS subunits as the distribution of neither the late endosomal Rab Vps21, the CORVET-specific subunit Vps3, the vacuolar SNARE Vam3 nor the late endosomal SNARE Pep12 changed under these conditions (Supplemental Figure S2). We concluded that Vps41 phosphorylation is crucial in dictating the localization of the entire HOPS complex.

The Vps41 S-A Mutant Accumulates Tubular Membrane Structures Adjacent to the Vacuole

We decided to analyze the ultrastructural changes caused by the Vps41 mutations. By EM, neither wild-type nor the cells expressing the Vps41 S-D mutant showed any significant alterations in their overall cell morphology (Figure 5, A and B). In the Vps41 S-A mutant, in contrast, we observed tubular, stacked membrane structures (Figure 5, C, D, G, and H), which were found proximal to the vacuole (Figure 5, F and I). However, the tubular structures were not as abundant and of the same large size as those detected in *yck3*Δ cells (Figure 1B). In this strain background, additional putative Yck3 substrates would lack phosphorylation and might contribute to enhanced phenotype of *yck3*Δ cells (Figure 1B) compared with the cells expressing the Vps41 S-A mutant (Figure 5).

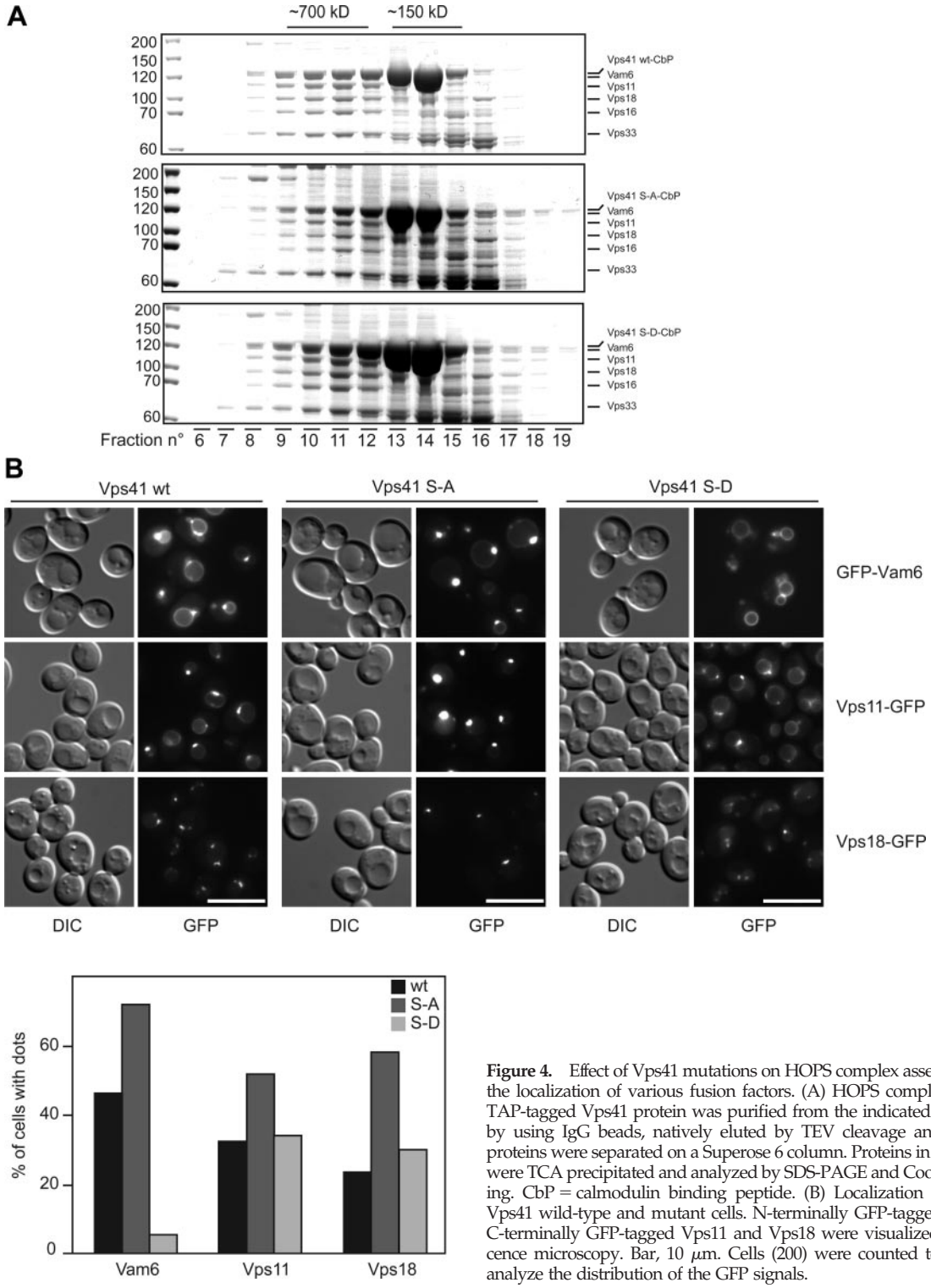

Figure 4. Effect of Vps41 mutations on HOPS complex assembly and on the localization of various fusion factors. (A) HOPS complex assembly. TAP-tagged Vps41 protein was purified from the indicated yeast strains by using IgG beads, natively eluted by TEV cleavage and the eluted proteins were separated on a Superose 6 column. Proteins in each fraction were TCA precipitated and analyzed by SDS-PAGE and Coomassie staining. CbP = calmodulin binding peptide. (B) Localization of tethers in Vps41 wild-type and mutant cells. N-terminally GFP-tagged Vam6 and C-terminally GFP-tagged Vps11 and Vps18 were visualized by fluorescence microscopy. Bar, 10 μm. Cells (200) were counted to statistically analyze the distribution of the GFP signals.

Vps41 Localization Is Linked to the Late Endosome

The morphological similarity between the tubules observed in the *yck3*Δ and the Vps41 S-A mutant (Figures 1B and 5), and the previously described class E endosomes (Rieder *et al*., 1996) prompted us to analyze the Vps41 localization in *vps27*Δ cells. Vps27 belongs to the ESCRT-0 complex involved in the generation of multivesicular bodies (Hurley and Emr, 2006). Interestingly, in wild-type cells Vps41-GFP redistributed partially from the vacuolar rim to the distinctive class E compartment of *vps27*Δ cells (Figure 6A), whereas GFP-Vam6 did not change its localization (Figure 6B). In the Vps41 S-A mutant, the dot accumulation of Vps41 was enhanced by the *VPS27* deletion but did not result in additional, distinct structures (Figure 6A, right). Likewise, GFP-Vam6 was confined to a single dot adjacent to vacuoles in the *vps27*Δ mutant, with a barely visible signal on the

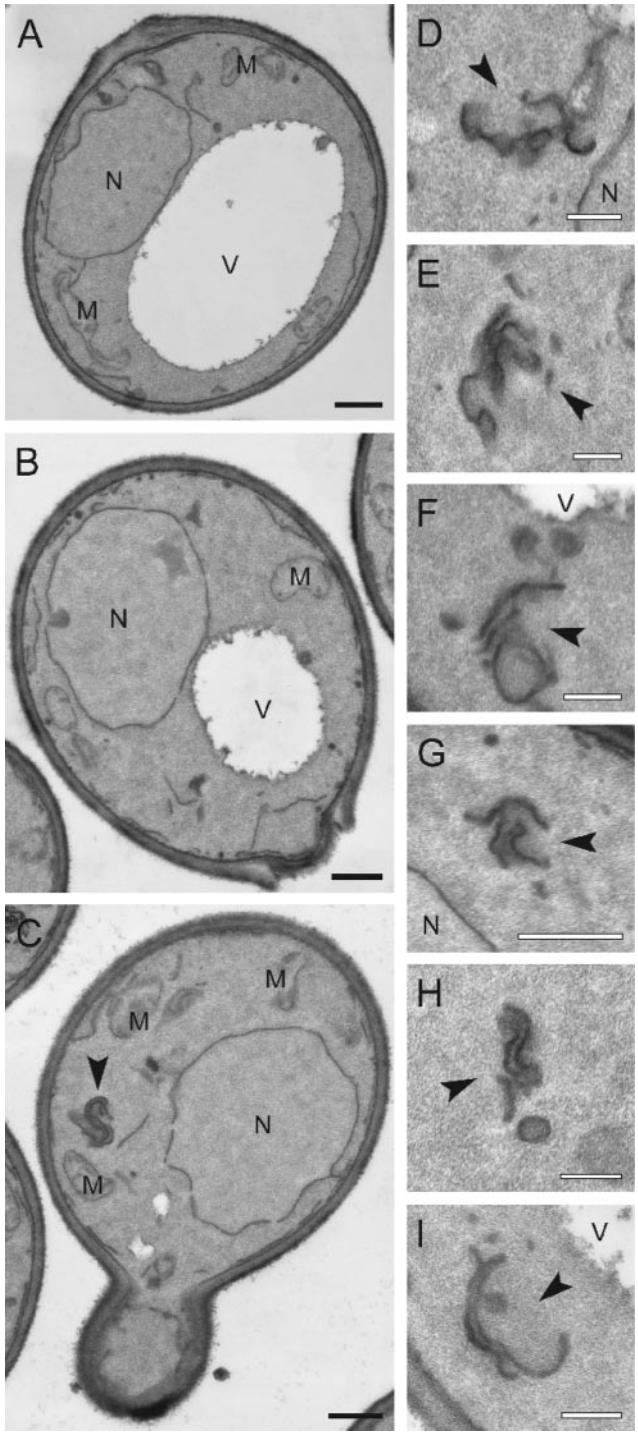

Figure 5. EM analysis of Vps41 mutant cells. The SEY6210 *vam2*Δ *NOP1*pr-*VPS41* wild-type (A), SEY6210 *vam2*Δ *NOP1*pr-*VPS41 S-D* (B), and SEY6210 *vam2*Δ *NOP1*pr-*VPS41 S-A* (C–I) strains were grown to exponential phase and embedded in Spurr's resin as described in *Materials and Methods*. Arrowheads in C–I highlight the clusters of membranes observed in cells expressing Vps41 S-A. N, nucleus; V, vacuole; M, mitochondrion; Black bar, 500 nm; white bar, 200 nm.

vacuolar limiting membrane. Vps41 S-A and Vam6 dots colocalized with the class E compartment labeled with FM4-64 (Figure 6, A and B), indicating that some Vam6 and Vps41 is also found on late endosomes, a distribution that becomes more apparent in the class E background. This finding is in agreement with previous results from our laboratory, which suggested that the endosomal CORVET tethering complex converts to the HOPS complex in the course of endosome maturation (Peplowska *et al*., 2007). This conversion is most likely required for efficient HOPS-dependent fusion of matured late endosomes with the vacuole. The cytosolic distribution of Vps41 S-D mutant was not influenced by the *VPS27* deletion but an increased vacuole fragmentation was observed (Supplemental Figure S3).

To test whether the puncta where Vps41 and Vam6 concentrate corresponds to an active fusion zone on the vacuole, we challenged vacuoles from the Vps41 S-A strain with high salt to induce fragmentation and monitored fusion upon removal of the salt stress (Bonangelino *et al*., 2002). When we followed vacuoles over time, we observed that they docked exclusively at zones with strongly enriched Vam6 (Figure 6C). This suggests that vacuoles contain a zone dedicated for fusion, which is enhanced by a block in Vps41 phosphorylation. This idea is also supported by in vitro data where an enrichment of fusion factors at docking zones has been previously reported during the vacuole-vacuole fusion assay (Wang *et al*., 2003). Our data, however, do not distinguish whether HOPS predefines such a zone, a concept that has to be clarified in future studies.

The Concentration of Vps41 S-A to Endosome–Vacuole Contact Zones Affects the AP-3 Pathway

Cargo proteins destined for the vacuole are transferred either directly from the Golgi to the vacuole by means of the vesicular AP-3 pathway, which is taken by the vacuolar SNAREs Vam3 and Nyv1, or reach the vacuole via the endosome. The latter pathway is used among others by the Prc1 (CPY) and Cps1 protein as well as Vam3 and Nyv1 if the AP-3 pathway is blocked. When we analyzed trafficking pathways to the vacuole in our mutant strains, we did not detect major defects in the transport of CPY or autophagic cargo, and we observed efficient sorting of Cps1 into the vacuolar lumen via multivesicular bodies (Supplemental Figure S4; our unpublished observations). We then followed the fate of a synthetic cargo of the AP-3 pathway—a fusion protein of the cytosolic domain of the vacuolar SNARE Nyv1 with the longer transmembrane domain of Snc1.This fusion protein lacks the Golgi-endosome targeting signal and hence is sorted to the plasma membrane if the AP-3 pathway is defective (Reggiori *et al*., 2000). This effect can be conveniently monitored by fluorescence microscopy. Although the Nyv1-Snc1 fusion protein arrived at the vacuole in cells with wild-type Vps41 or the S-D mutation, some fusion protein was also observed on the plasma membrane in cells expressing Vps41 S-A or lacking Yck3 (Figure 7). This indicates that the AP-3 pathway is impaired under these conditions. Defective protein sorting via the AP-3 pathway in yck3Δ cells has also been observed by Anand *et al*. (2009). We suggest that the strong accumulation of Vps41 S-A to the distinct fusion "hot spot" on the vacuole—where it can function in the fusion with late endosomes and other vacuoles—restricts its availability for the AP-3 pathway. Alternatively, is possible that only phosphorylated Vps41 is required in the AP-3 pathway.

Nonphosphorylated Vps41 Confers Fusion Resistance to a GTPase-activating Protein

We previously showed that the in vitro vacuole fusion sensitivity to Ypt7 inhibitors is reduced if Yck3 was lacking from cells (LaGrassa and Ungermann, 2005). If this effect is

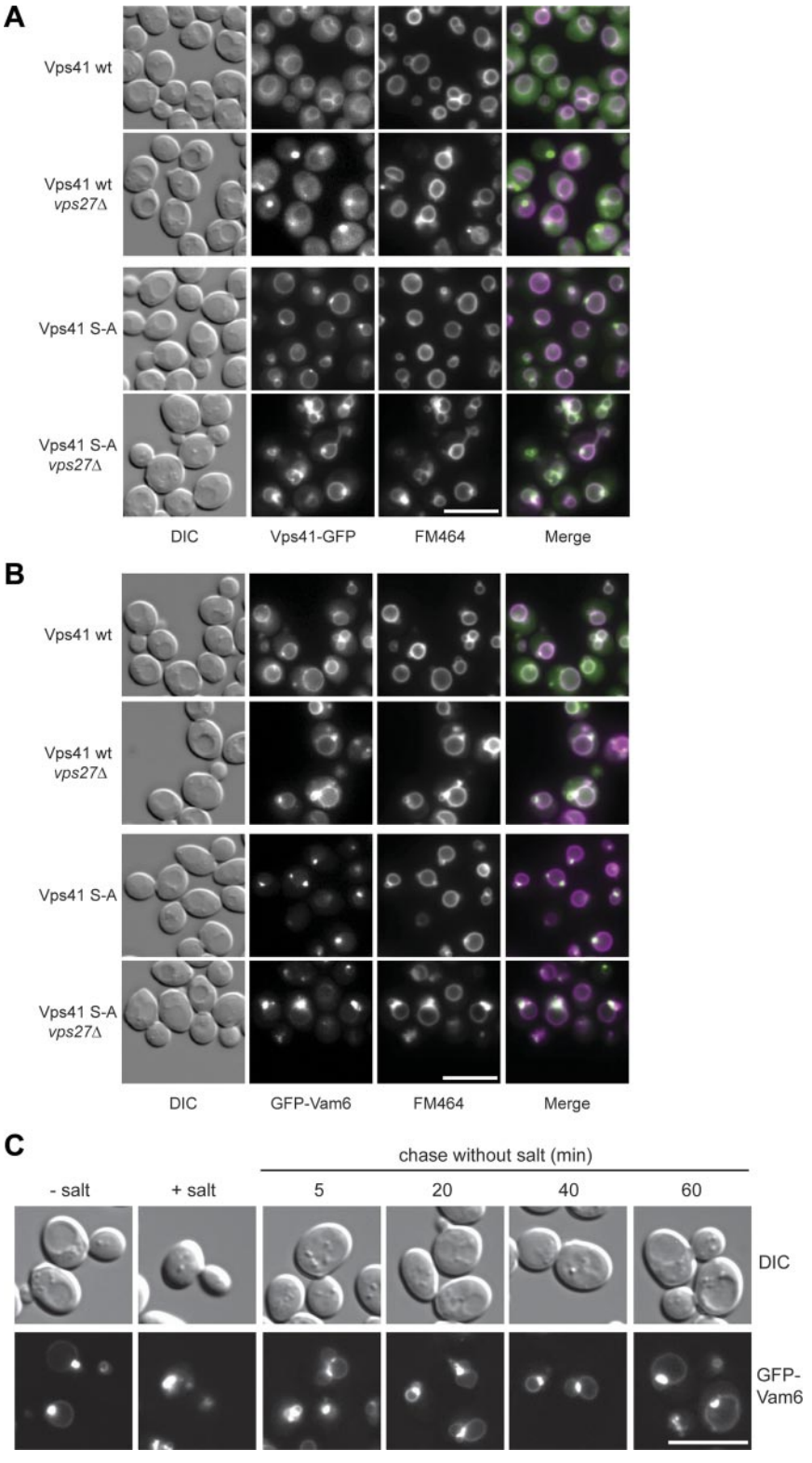

Figure 6. Nonphosphorylated Vps41 and Vam6 are enriched at vacuole fusion sites. (A) Localization of Vps41-GFP in *vps27*Δ strain. SEY6210 cells expressing C-terminal GFP-tagged wild-type and mutant (S-A) Vps41 were labeled with FM4-64 and analyzed by fluorescence microscopy. Where indicated, *VPS27* was deleted. Bar, 10 μm. (B) Localization of GFP-Vam6 in the *vps27*Δ strain. SEY6210 wild-type and *vps27*Δ cells expressing N-terminal GFP-tagged Vam6 in the respective Vps41 background were incubated with FM4-64 and analyzed by fluorescence microscopy. Bar, 10 μm. (C) In vivo fusion of vacuoles after relieve from high salt concentration stress. Cells expressing the Vps41 S-A mutant and the N-terminally GFP-tagged Vam6 fusion were incubated with 0.4 M NaCl for 30 min, followed by a wash with YPD medium and grown for the indicated times. Localization of Vam6 and vacuole morphology were monitored by fluorescence microscopy. Bar, 10 μm.

linked to Vps41 phosphorylation, the Vps41 S-A mutant should mirror the *yck3*Δ mutant in the vacuole fusion assay. We generated fusion tester vacuoles carrying this Vps41 mutant form. Vacuole fusion was then monitored using isolated vacuoles from the two tester strains in the established content mixing assay (Haas, 1995). Fusion of *yck3*Δ and the S-A strains was comparable with wild-type fusion (data not shown). The active GAP domain of Gyp1 has been successfully used as a Rab-specific inhibitor of in vitro vacuole fusion and can block vacuole fusion to the same extend as the Ypt7 GAP Gyp7 (Merz and Wickner, 2004; Brett *et al*., 2008). If the active GAP-domain of Gyp1 was titrated into

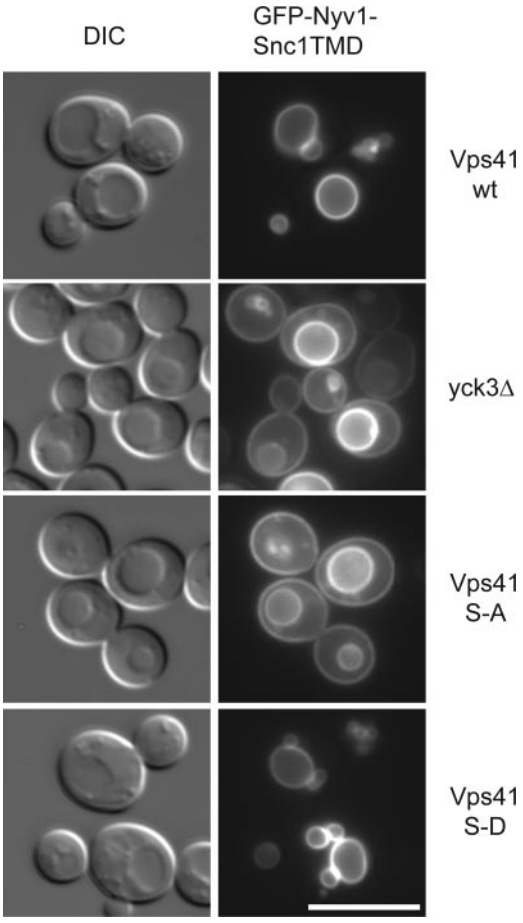

Figure 7. The AP-3 pathway is impaired in the Vps41 S-A mutant. Localization of GFP-Nyv1-Snc1TMD in Vps41 wild-type and mutant cells. Cells expressing GFP-tagged Nyv1-Snc1TMD in the indicated Vps41 backgrounds were visualized by fluorescence microscopy. Bar, 10 μm.

the fusion assay, we observed strong inhibition of wild-type vacuoles, whereas vacuoles carrying Vps41 S-A and *yck3*Δ vacuoles were clearly less sensitive (Figure 8A). This indicates that the GAP enzyme cannot access Ypt7 efficiently under these conditions, because the fusion of *yck3*Δ vacuoles is still inhibited by Ypt7 antibodies and therefore Ypt7-dependent (LaGrassa and Ungermann, 2005).

Ypt7 Overproduction Can Counteract the Effects of Vps41 Phosphorylation

We then asked whether alteration in the Ypt7 cycle would affect the vacuolar morphology of the different Vps41 mutants. When we tagged Ypt7 N-terminally with GFP and monitored its localization, we detected the protein on vacuoles in wild-type cells as expected (Figure 8B). In the S-A mutant, Ypt7 also accumulated in dots on the vacuolar rim. In contrast, GFP-tagging of Ypt7 in the Vps41 S-D background resulted in a complete vacuole fragmentation. This effect is only evident in combination with the S-D mutation. Our data suggest that the mislocalization of Vps41 S-D together with a Ypt7 protein affected in its functionality by the N-terminal GFP-tag leads to an in vivo fusion defect that is reflected by vacuole fragmentation. If this interpretation was correct, then the untagged Ypt7 should compensate for this defect. This was indeed the case. Overexpression of untagged Ypt7 wild-type rescues the vacuole fragmentation phenotype of the S-D mutant (Figure 8C). Moreover, we observed that more Vps41 S-D localized to the vacuolar rim and prevacuolar dots under these conditions (Figure 8C). We conclude that Vps41 does not solely depend on the Yck3 phosphorylation site for its localization but that it also harbors a Ypt7 interaction site, which supports its binding to the endosomal and vacuolar membrane in vivo. If more Ypt7 is provided, the localization defect of Vps41 caused by the phosphomimetic mutation and consequently the vacuole morphology defect are rescued (Figure 8C). In complete agreement with this interpretation, the in vitro binding between purified Vps41 and Ypt7 has recently been demonstrated (Brett *et al*., 2008; Ostrowicz and Ungermann, unpublished data).

In Vivo Ypt7 Accessibility Depends on the Phosphorylation Status of Vps41

Two additional factors have been implicated in the control of Ypt7: Vam6 has GEF activity (Wurmser *et al*., 2000), whereas Gyp7 has been identified as a Ypt7-specific GAP, whose activity leads to Ypt7 inactivation and subsequent Gdi1-dependent release from the vacuole (Albert and Gallwitz, 1999). Consequently, we used an overexpression approach to test the effect of Gyp7 on vacuole morphology in the Vps41 mutant backgrounds (Figure 8D). To facilitate the construction of our strain, we generated diploid cells, in which only one copy of Ypt7 is tagged and monitored vacuole morphology by following GFP-Ypt7 and FM4-64 labeling.

For Gyp7 overexpression, we expected an inactivation of Ypt7 and subsequent vacuole fragmentation. This was to some extent the case for cells with wild-type Vps41 and the S-D mutant (Figure 8D). Additionally, we observed Ypt7 redistribution to the cytosol. In contrast, cells expressing Vps41 S-A maintained some Ypt7 associated to the vacuoles and were less responsive to the GAP overproduction (Figure 8D), in complete agreement with the reduced sensitivity in vitro (Figure 8A). Together, only the Vps41 S-A mutant efficiently counteracted the effects of Gyp7 overproduction on the Ypt7 distribution and the vacuole morphology. We assume that this protein variant is more prone to interact with Ypt7 because it binds more efficiently to membranes. Therefore, the Vps41 S-A mutant most likely blocks the access of Gyp7 to Ypt7, which explains the reduced response of this mutant. In combination, our data imply that Vps41 has two binding sites on membranes, which regulate its function: one binding site that is influenced by Yck3-mediated phosphorylation, as well as a Ypt7-dependent binding site.

DISCUSSION

Protein phosphorylation modulates multiple events along the endocytic and exocytic pathways: coat polymerization, membrane tethering, and SNARE assembly (Langer *et al*., 2007; Preisinger and Barr, 2005). Here, we have analyzed how phosphorylation of Vps41 can control its function in the tethering stage at the endosome/vacuole interface. The phosphorylation site found in Vps41 resembles the casein kinase 1 consensus phosphorylation site: S/T(P)-X_{1-2}-S/T, where the upstream phosphorylation in residue S364 most probably provides the negative charge required for molecular recognition by the Yck3 kinase (Gross and Anderson, 1998). The identification of the Vps41 phosphorylation sites allowed us to separate Vps41-regulation from Yck3-dependent phosphorylation effects on additional targets within the

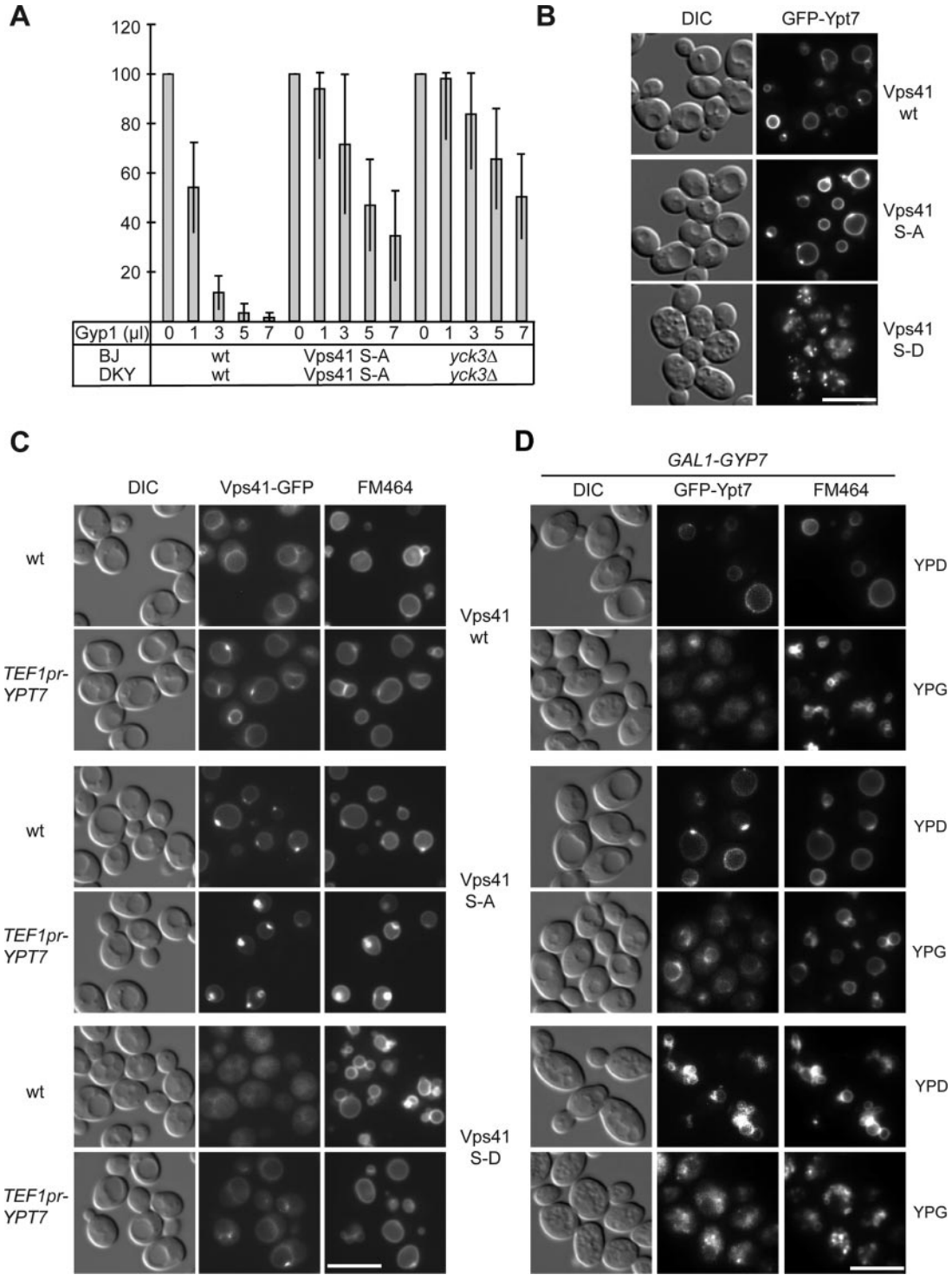

Figure 8. Vps41 phosphorylation is linked to Rab Ypt7 cycle. (A) Sensitivity of vacuole fusion to Gyp1. Standard fusion reactions containing BJ and DKY vacuoles from the indicated strains were incubated for 90 min with or without ATP and increasing amounts of Gyp1. Fusion activity was determined as described in *Materials and Methods*. Fusion is set to 100% for untreated cells. OD_{400} was 0.54 ± 0.07 for wild-type, 0.41 ± 0.08 for *yck3*Δ cells, and for vacuoles expressing Vps41 S-A, 0.47 ± 0.07. (B) GFP-Ypt7 localization in the Vps41 mutants. Strains carrying N-terminal GFP-tagged Ypt7 were visualized by DIC and fluorescence microscopy. Bar, 10 μm. (C) Effect of Ypt7 overproduction on Vps41 localization. Cells expressing Ypt7 under the *TEF* promoter and C-terminally GFP-tagged Vps41 or mutants were analyzed by fluorescence microscopy. (D) Ypt7 inactivation triggered by Gyp7 overproduction. Diploid strains containing GFP-tagged Ypt7 and Vps41 wt or the indicated mutants were grown in YPD or YPG to induce Gyp7-overproduction. Vacuoles were stained with FM4-64 and visualized in the fluorescence microscope. Bar, 10 μm.

cell, in particular other proteins of the endosomal system. For example, the vacuolar SNARE Vam3 has been identified as an additional Yck3 substrate (Brett *et al*., 2008), but the phosphorylation site remains to be determined. Our data

suggest that nonphosphorylated Vps41, presumably as part of the HOPS complex, is concentrated in dot-like structures that correspond to the fusion site between late endosomes and the vacuole. In fact, Vam6/Vps39 and Vps41 get even stronger enriched at this site if the ESCRT-0 subunit Vps27 was deleted. Thus, it is likely that the HOPS complex is also temporarily present on late endosomes to support fusion with the vacuole. This finding confirms previous studies in our laboratory, which provided evidence that formation of the HOPS complex can occur upon subunit exchange of the homologous endosomal CORVET tethering complex (Peplowska *et al*., 2007). The conversion occurs most likely in the course of endosomal maturation, a feature that was previously shown for the corresponding Rabs on single endosomes in higher eukaryotic cells (Rink *et al*., 2005). Interestingly, only the Rab5 GTPase Vps21, but not the CORVET subunits Vps3 or Vps8, is enriched in the class E compartment (our unpublished observations), suggesting once more that the tether conversion is taking place during endosome maturation. Our ultrastructural analysis reveals that cells carrying the nonphosphorylated Vps41 mutant behave very similar to *yck3*Δ cells and accumulate tubular endosomal structures close to the vacuole. The reason for this accumulation is not yet clear, but it is most likely a consequence of reduced recycling due to impaired mobility of Vps41 under these conditions.

Our analysis of the Vps41 phosphorylation site also sheds light on the dynamics of the HOPS complex. All HOPS subunits analyzed were concentrated together with Vps41 at the endosome-vacuole fusion site in the nonphosphorylated Vps41 S-A mutant. In the Vps41 S-D background, in contrast, Vps41 was found to a large extent in the cytoplasm, whereas Vps11, Vps18, and Vam6 were less accumulated in dots, but still present on the vacuolar rim. This suggests that Vps41 can operate independently from the remaining HOPS subunits and could act in the recruitment of the HOPS subunits to the endosome-vacuole fusion site. Interestingly, we were able to purify assembled HOPS complex in all Vps41 background strains (Figure 4A), although we cannot exclude slight changes in the efficiency of HOPS assembly. It is therefore possible that only the unassembled Vps41 undergoes the phosphorylation-dependent dynamics that are mimicked by our mutations.

We also observed that the transport of AP-3 cargo is impaired in cells lacking Vps41 phosphorylation in agreement with Anand *et al*. (2009). This suggests a positive feedback regulation: Yck3, sorted to the vacuole via AP-3 vesicles (Sun *et al*., 2004), is required to release Vps41 from this endosomal docking site and make it available for budding and fusion of AP-3 vesicles, which apparently dock at a different site on vacuoles. A potential phosphorylation of Vps41 on AP-3 vesicles might be without consequences as Vps41 was proposed to be part of the AP-3 coat (Rehling *et al*., 1999).

We do not yet completely understand how phosphorylation of Vps41 affects its function. The phosphorylation site is located within an insertion of the putative N-terminal β-propeller of Vps41 (Lu *et al*., 2007). This insertion corresponds most likely to a loop between two β-sheets within the β-propeller (http://bioinf.cs.ucl.ac.uk/psipred/). Potentially, phosphorylation of this loop disrupts a binding site of Vps41 at the endosome–vacuole interface and thereby liberates Vps41 and the HOPS complex. We did not observe any significant alteration in the HOPS complex assembly or Ypt7 binding in vitro caused by mutating the phosphorylation site of Vps41 (Figure 4A; our unpublished observations). It is therefore unlikely that Vps41 uses this loop to interact with the HOPS complex or Ypt7 directly. The elucidation of the binding mode of the Vps41-loop will be an important future task.

In addition to the loop containing the phosphorylation site, which can mediate membrane binding, Vps41 contains a Ypt7 binding site (Brett *et al*., 2008; Ostrowicz and Ungermann, unpublished data). In agreement with this notion, we observed that overexpression of Ypt7 rescues the vacuole morphology defect and localization of the Vps41 S-D mutant. Furthermore, interfering with Ypt7 function or with its active levels in combination with constitutive Vps41 phosphorylation enhances the vacuole fragmentation phenotype. We conclude that both binding sites are required for efficient and dynamic Vps41 localization and thus the HOPS complex function in wild-type cells. The constitutively unphosphorylated Vps41 variant does not exhibit vacuole fragmentation upon Gyp7 overproduction. We assume that the efficient binding of the nonphosphorylated Vps41 to membranes results in a higher probability to interact with Ypt7, leading to a limited accessibility of Ypt7. Moreover, Ypt7 inactivation by Gyp7 might have only a weak effect, because Vps41 and the HOPS complex do still efficiently localize independently of Ypt7. The analysis of the Gyp7 recruitment to membranes is needed to clarify, how Vps41 S-A can prevent efficient Gyp7 action.

Our data provide evidence for a role of Vps41 and the HOPS complex at late endosomes. It is possible that the loading of Ypt7 onto late endosomes and the recruitment of the HOPS complex are controlled by Vps41, which in turn is governed by Yck3. It will be important to investigate, how Vps41 phosphorylation and Ypt7 activation are regulated in concert and how Yck3 activity is controlled on yeast vacuoles.

ACKNOWLEDGMENTS

We thank all members of the Ungermann group for discussion, J. Heinisch for antibodies, and Angela Perz and Nadine Decker (BZH) for technical support. This work was funded by the Deutsche Forschungsgemeinschaft (SFB431, CA806/2-1), the Fundación Ramón Areces (to M. C.), and the Hans-Mühlenhoff foundation (to C. U.). F. R. is supported by the Netherlands Organization for Health Research and Development (ZonMW-VIDI-917.76.329) and by the Utrecht University (High Potential grant).

REFERENCES

Albert, S., and Gallwitz, D. (1999). Two new members of a family of Ypt/Rab GTPase activating proteins. Promiscuity of substrate recognition. J. Biol. Chem. *274*, 33186–33189.

Anand, V. C., Daboussi, L., Lorenz, T. C., and Payne, G. S. (2009). Genome-wide analysis of AP-3 dependent protein transport in yeast. Mol. Biol. Cell *20*, 1592–1604.

Bonangelino, C. J., Nau, J. J., Duex, J. E., Brinkman, M., Wurmser, A. E., Gary, J. D., Emr, S. D., and Weisman, L. S. (2002). Osmotic stress-induced increase of phosphatidylinositol 3,5-bisphosphate requires Vac14p, an activator of the lipid kinase Fab1p. J. Cell Biol. *156*, 1015–1028.

Bos, J. L., Rehmann, H., and Wittinghofer, A. (2007). GEFs and GAPs: critical elements in the control of small G proteins. Cell *129*, 865–877.

Brett, C. L., Plemel, R. L., Lobinger, B. T., Vignali, M., Fields, S., and Merz, A. J. (2008). Efficient termination of vacuolar Rab GTPase signaling requires coordinated action by a GAP and a protein kinase. J. Cell Biol. *182*, 1141–1151.

Cai, H., Reinisch, K., and Ferro-Novick, S. (2007). Coats, tethers, Rabs, and SNAREs work together to mediate the intracellular destination of a transport vesicle. Dev. Cell *12*, 671–682.

Drin, G., Morello, V., Casella, J. F., Gounon, P., and Antonny, B. (2008). Asymmetric tethering of flat and curved lipid membranes by a golgin. Science *320*, 670–673.

Griffith, J., Mari, M., De Maziere, A., and Reggiori, F. (2008). A cryosectioning procedure for the ultrastructural analysis and the immunogold labelling of yeast *Saccharomyces cerevisiae*. Traffic *9*, 1060–1072.

Gross, S. D., and Anderson, R. A. (1998). Casein kinase I: spatial organization and positioning of a multifunctional protein kinase family. Cell Signal. *10*, 699–711.

Haas, A. (1995). A quantitative assay to measure homotypic vacuole fusion in vitro. Methods Cell Sci. *17*, 283–294.

Hurley, J. H., and Emr, S. D. (2006). The ESCRT complexes: structure and mechanism of a membrane-trafficking network. Annu. Rev. Biophys. Biomol. Struct. *35*, 277–298.

Janke, C., *et al*. (2004). A versatile toolbox for PCR-based tagging of yeast genes: new fluorescent proteins, more markers and promoter substitution cassettes. Yeast *21*, 947–962.

LaGrassa, T. J., and Ungermann, C. (2005). The vacuolar kinase Yck3 maintains organelle fragmentation by regulating the HOPS tethering complex. J. Cell Biol. *168*, 401–414.

Langer, J. D., Stoops, E. H., Bethune, J., and Wieland, F. T. (2007). Conformational changes of coat proteins during vesicle formation. FEBS Lett. *581*, 2083–2088.

Lu, S., Suzuki, T., Iizuka, N., Ohshima, S., Yabu, Y., Suzuki, M., Wen, L., and Ohta, N. (2007). Trypanosoma brucei vacuolar protein sorting 41 (VPS41) is required for intracellular iron utilization and maintenance of normal cellular morphology. Parasitology *134*, 1639–1647.

Markgraf, D. F., Peplowska, K., and Ungermann, C. (2007). Rab cascades and tethering factors in the endomembrane system. FEBS Lett. *581*, 2125–2130.

Mayer, A., Wickner, W., and Haas, A. (1996). Sec18p (NSF)-driven release of Sec17p (alpha-SNAP) can precede docking and fusion of yeast vacuoles. Cell *85*, 83–94.

Merz, A. J., and Wickner, W. T. (2004). Trans-SNARE interactions elicit Ca2+ efflux from the yeast vacuole lumen. J. Cell Biol. *164*, 195–206.

Nakamura, N., Hirata, A., Ohsumi, Y., and Wada, Y. (1997). Vam2/Vps41p and Vam6/Vps39p are components of a protein complex on the vacuolar membranes and involved in the vacuolar assembly in the yeast *Saccharomyces cerevisiae*. J. Biol. Chem. *272*, 11344–11349.

Ostrowicz, C. W., Meiringer, C. T., and Ungermann, C. (2008). Yeast vacuole fusion: a model system for eukaryotic endomembrane dynamics. Autophagy *4*, 5–19.

Peplowska, K., Markgraf, D. F., Ostrowicz, C. W., Bange, G., and Ungermann, C. (2007). The CORVET tethering complex interacts with the yeast Rab5 homolog Vps21 and is involved in endo-lysosomal biogenesis. Dev. Cell *12*, 739–750.

Preisinger, C., and Barr, F. A. (2005). Kinases regulating Golgi apparatus structure and function. Biochem. Soc. Symp. 15–30.

Puig, O., Rutz, B., Luukkonen, B. G., Kandels-Lewis, S., Bragado-Nilsson, E., and Seraphin, B. (1998). New constructs and strategies for efficient PCR-based gene manipulations in yeast. Yeast *14*, 1139–1146.

Raymond, C. K., Howald-Stevenson, I., Vater, C. A., and Stevens, T. H. (1992). Morphological classification of the yeast vacuolar protein sorting mutants: evidence for a prevacuolar compartment in class E vps mutants. Mol. Biol. Cell. *3*, 1389–1402.

Reggiori, F., Black, M. W., and Pelham, H. R. (2000). Polar transmembrane domains target proteins to the interior of the yeast vacuole. Mol. Biol. Cell. *11*, 3737–3749.

Rehling, P., Darsow, T., Katzmann, D. J., and Emr, S. D. (1999). Formation of AP-3 transport intermediates requires Vps41 function. Nat. Cell Biol. *1*, 346–353.

Rieder, S. E., Banta, L. M., Kohrer, K., McCaffery, J. M., and Emr, S. D. (1996). Multilamellar endosome-like compartment accumulates in the yeast vps28 vacuolar protein sorting mutant. Mol. Biol. Cell. *7*, 985–999.

Rieder, S. E., and Emr, S. D. (1997). A novel RING finger protein complex essential for a late step in protein transport to the yeast vacuole. Mol. Biol. Cell. *8*, 2307–2327.

Rigaut, G., Shevchenko, A., Rutz, B., Wilm, M., Mann, M., and Seraphin, B. (1999). A generic protein purification method for protein complex characterization and proteome exploration. Nat. Biotechnol. *17*, 1030–1032.

Rink, J., Ghigo, E., Kalaidzidis, Y., and Zerial, M. (2005). Rab conversion as a mechanism of progression from early to late endosomes. Cell *122*, 735–749.

Seals, D. F., Eitzen, G., Margolis, N., Wickner, W. T., and Price, A. (2000). A Ypt/Rab effector complex containing the Sec1 homolog Vps33p is required for homotypic vacuole fusion. Proc. Natl. Acad. Sci. USA *97*, 9402–9407.

Starai, V. J., Hickey, C. M., and Wickner, W. (2008). HOPS Proofreads the trans-SNARE Complex for Yeast Vacuole Fusion. Mol. Biol. Cell. *19*, 2500–2508.

Stroupe, C., Collins, K. M., Fratti, R. A., and Wickner, W. (2006). Purification of active HOPS complex reveals its affinities for phosphoinositides and the SNARE Vam7p. EMBO J. *25*, 1579–1589.

Sun, B., Chen, L., Cao, W., Roth, A. F., and Davis, N. G. (2004). The yeast casein kinase Yck3p is palmitoylated, then sorted to the vacuolar membrane with AP-3-dependent recognition of a YXXPhi adaptin sorting signal. Mol. Biol. Cell. *15*, 1397–1406.

Wang, L., Merz, A. J., Collins, K. M., and Wickner, W. (2003). Hierarchy of protein assembly at the vertex ring domain for yeast vacuole docking and fusion. J. Cell Biol. *160*, 365–374.

Whyte, J. R., and Munro, S. (2002). Vesicle tethering complexes in membrane traffic. J. Cell Sci. *115*, 2627–2637.

Wurmser, A. E., Sato, T. K., and Emr, S. D. (2000). New component of the vacuolar class C-Vps complex couples nucleotide exchange on the ypt7 GTPase to SNARE-dependent docking and fusion. J. Cell Biol. *151*, 551–562.